Article

Optical Vortex Beam for Gentle and Ultraprecise Intrastromal Corneal Dissection in Refractive Surgery

Sebastian Freidank[1], Alfred Vogel[1], and Norbert Linz[1]

[1] Institute of Biomedical Optics, University of Luebeck, Luebeck, Germany

Purpose: We introduce a novel focus shaping concept for intrastromal corneal dissection that facilitates cleavage along corneal lamellae, and we analyze laser–tissue interactions governing cutting effectiveness and mechanical side effects.

Methods: Focus shaping was achieved by a spiral phase plate that converts an incident Gaussian beam into a Laguerre–Gaussian beam with a helical phase. Such vortex beams have zero intensity at their center, are propagation invariant, and possess a ring focus equal in length to the Gaussian focus but with a larger diameter. Cutting precision and the required absorbed energy for flap dissection were compared for Gaussian and vortex beams on ex vivo porcine corneal specimens at pulse durations between 480 fs and 9 ps. Cutting quality and bubble formation were characterized by scanning electron microscopy and macro photography.

Results: With the vortex beam, the cuts were much smoother. Bubble formation was markedly reduced because cutting can be performed close to the bubble threshold, whereas with the Gaussian beam energies well above threshold are needed. Although the incident energy at the flap dissection threshold was slightly larger for the vortex beam, the absorbed energy was much smaller and contributed more effectively to cutting. This reduced plasma-induced pressure more than sevenfold.

Conclusions: The vortex beam approach for corneal dissection is a simple, versatile, and cost-effective way of improving the precision of refractive surgery while reducing bubble formation and pressure-related mechanical side effects.

Translational Relevance: Phase plates for propagation invariant vortex beams are easily implemented in the beam path of next-generation clinical devices.

Introduction

Femtosecond laser-assisted in situ keratomileusis (LASIK) was introduced in the 1990s[1–5] and is a well-established method to correct refractive errors such as hyperopia, myopia, or astigmatism in the human eye; more than 18 million operations have been reported worldwide.[6–9] A decade ago, small incision lenticule extraction (SMILE) was introduced.[10] Here, a small lenticule is dissected within the corneal stroma and removed through a small side cut to correct the refractive error in one step using only the infrared (IR) femtosecond (fs) laser system. This flapless approach improves the postsurgical structural stability of the cornea and has been shown to reduce some of the side

effects in refractive surgery.[11,12] It can be performed with one laser system, whereas in LASIK flap dissection is followed by application of excimer laser pulses for ablative reshaping of the corneal stroma. Recently, a novel approach for hyperopia correction based on dissection of an intrastromal pocket followed by the injection of a biocompatible filler material has been introduced.[13,14]

Despite more than 20 years of experience with LASIK and SMILE, there is still room for improvement with regard to efficiency, precision, and safety. Significant improvements can be achieved by addressing the key step of the refractive laser procedure: intrastromal dissection. In most clinical systems, IR fs laser pulses with pulse energies between 0.3 and 1.6 µJ are focused into the corneal stroma at a numerical
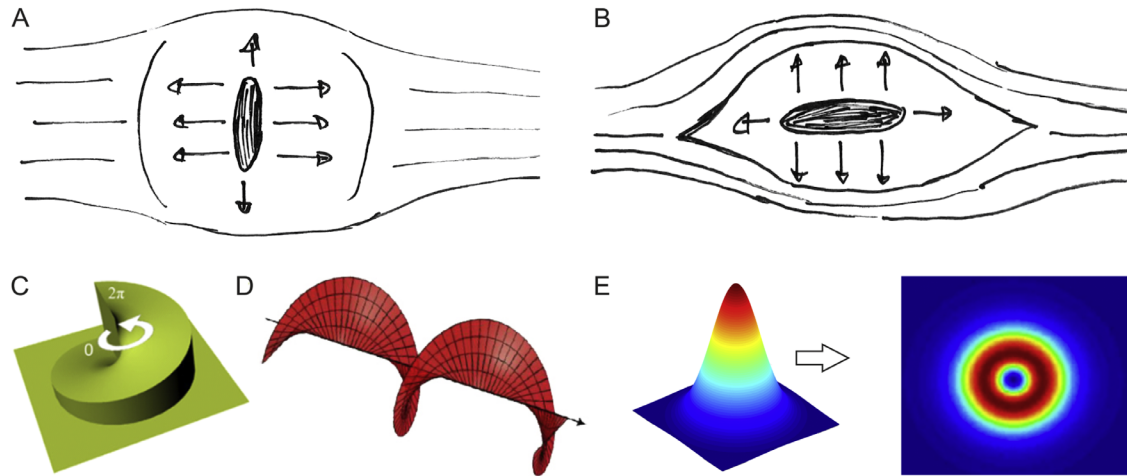
Figure 1. Schematic drawing of the elongated laser plasma of a Gaussian beam in side view, roughly indicating the direction of mechanical forces leading to cavity formation within the corneal lamellae (**A**). To improve cutting precision, it would be ideal to have a disk-like plasma orientated parallel to the corneal surface along the cutting direction and the cleavage lines given by corneal lamellae (**B**). This feature can be approximated by introducing a spiral phase mask with 2π phase shift (**C**) into the beam path that converts the linear polarized Gaussian beam exiting the laser into a vortex beam with helical phase (**D**). The foci of the Gaussian and vortex beam are presented in (**E**), with the vortex beam focus shown in the top view. It has a ring shape, with the same length in the axial direction as the focus of the Gaussian beam, but with a diameter two times larger.[22]

aperture (NA) of 0.3 to 0.4 in a raster pattern with 3 to 6.5 μm spot separation.[15] Dissection is based on laser-induced plasma formation followed by a rapidly expanding shock wave and cavitation bubble.[16–19] The creation of an intrastromal cut relies only partly on tissue vaporization but mainly on the thermomechanical interaction of the plasma shock wave and cavitation bubble with the layered corneal tissue that leads to a cleavage of corneal lamellae.[4,19]

However, cutting precision is compromised by the elongated shape of the laser plasma, which is oriented along the optical axis, perpendicular to the desired cutting direction. The diameter (d) and length (l) of the elongated focus are given by Abbe's equations: $d = \lambda/\text{NA}$ and $l = 4\,(\lambda/\text{NA}^2)$.[20] The ratio l/d for parameters used in clinical systems for flap cutting is approximately 10.5. To improve the dissection process, it would be ideal to be able to rotate the "laser knife" such that the blade is oriented in cutting direction as shown schematically in Figures 1A and 1B. Unfortunately, the fundamental laws of optics do not allow this, but one can try to come as close as possible to achieving this simple concept.

In this paper, we introduce a new concept of focus shaping for gentle and ultraprecise intrastromal dissection in refractive surgery that is based on the idea presented in Figure 1. A spiral phase plate with phase shift of 2π is used to convert the Gaussian beam into a helically phased vortex beam. The helical phase results in destructive interference at the center, where the phase

difference between beam parts from opposite sides of the beam is always π (i.e., half of the wavelength of light). This feature is propagation invariant; therefore, the laser focus has a ring shape. The focus length in axial direction remains the same as for the Gaussian beam, but the diameter is two times larger.[22,23] The larger aspect ratio between plasma diameter and length facilitates cleavage along the corneal lamellae and enables dissection with lower plasma energy density and less bubble formation, resulting in smoother cuts.[24] A detailed analysis of the underlying laser tissue interactions shows that this goes along with a significant reduction of mechanical side effects. Gentler dissection and reduced intrastromal deformation by residual bubbles may improve the safety and precision of both LASIK and SMILE.

Methods

Experiments were performed in ex vivo porcine eyes. We have taken flap cutting as an example for an intrastromal dissection procedure that is relevant for both LASIK and SMILE, because the dissection quality can be readily assessed by evaluating the ease of flap lifting. We first determined the energy required for flap cutting for IR Gaussian and vortex beams. Pulse durations were varied from 480 fs to 9 ps to evaluate the influence of pulse length on

cutting energy and precision for the novel approach (vortex beam) compared with the established technique (Gaussian beam). Second, the cutting quality was characterized by microscopic imaging and scanning electron microscopy. Finally, transmission measurements during flap cutting were employed to demonstrate that the plasma energy density can be significantly reduced by focus shaping.

Cornea Specimens

The study was performed on ex vivo corneas obtained from fresh (<4 hours postmortem) porcine eyes. After enucleation, the eyes were stored at 8°C in nutrient solution (Dulbecco's Modified Eagle's Medium–low glucose; Sigma-Aldrich, St. Louis, MO). Immediately before the experiment, the epithelial layer of the cornea was removed, the cornea was excised by a cut close to the corneal limbus, and an 8-mm biopsy punch (BP-80F; KAI Medical Laboratory, Dallas, TX) was used to prepare the circular specimen. The cornea specimen was then transferred into a custom-designed holder with exchangeable cover glasses on the front and back sides that flattened the cornea during dissection.

Laser System and Beam Delivery

We used a fiber-laser-based chirped pulse amplification system with 1030-nm wavelength and a tunable pulse duration for dissection of the corneal flap (Cazadero; Calmar Laser, Palo Alto, CA). We employed pulse durations of 480 fs, 3 ps, and 8.8 ps. The beam quality parameter of the fiber laser system was specified by the manufacturer as $M^2 < 1.2$. The laser pulse shape and laser pulse duration were characterized by use of an autocorrelator (pulseCheck; APE, Berlin, Germany). A schematic drawing of the experimental setup is shown in Figure 2.

To convert the linear polarized Gaussian beam into a helically phased Laguerre–Gaussian vortex beam, a fused-silica spiral phase plate with maximum phase shift $\Delta\varphi = 2\pi$ (VL-209-I-Y-A, vortex grade A; HOLO/OR Ltd., Ness Ziona, Israel) was inserted into the beam path. Because the phase plate is produced by etching, it consists of 16 segments with stepwise increasing $\Delta\varphi$. By passing the phase plate, the laser beam is converted into a Laguerre–Gaussian vortex beam of order $m = 1$. The focus has a ring shape, with the same length in the axial direction as the focus of the Gaussian beam but a diameter that is two times larger, as shown in Figures 1C to 1E.[22]

Laser pulses with Gaussian and Laguerre–Gaussian shapes were focused through a microscope objective (Objective LD Plan-Neofluar, 63×, NA 0.75; Carl Zeiss
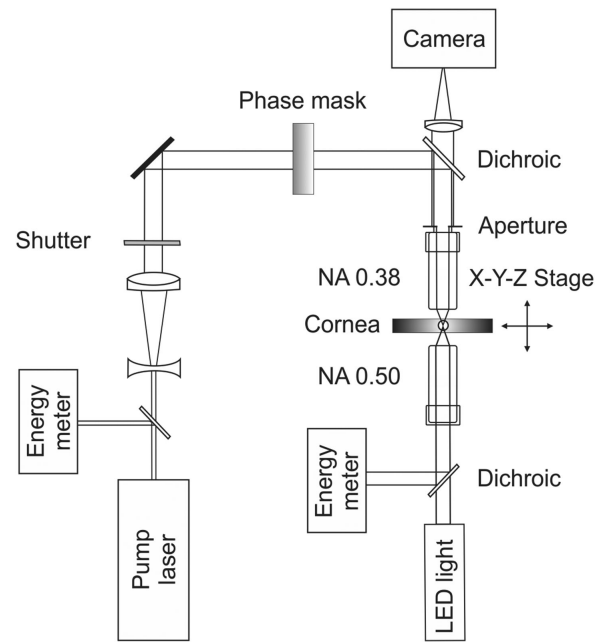

Figure 2. Experimental setup for the investigation of intrastromal laser dissection.

Microscopy, White Plains, NY) into the cornea. The numerical aperture was reduced to 0.38 by means of an aperture in the rear entrance pupil to mimic focusing conditions in clinical flap and lenticule dissection. Assuming $M^2 = 1.1$, the corresponding focus diameters are $d_{Gauss} = 3.0$ μm for the clipped Gaussian beam and $d_{ring} = 6.0$ μm for the vortex beam (factor 2).[20,22] Pulses were applied in a raster pattern with 6-μm spot separation. For this purpose, the laser was run at a 5-kHz repetition rate, and the porcine cornea was continuously moved by means of a three-dimensional translation stage at 30 mm/s translation velocity adjusted to the repetition rate. The flap bed was cut at 150-μm depth within a circular area 6 mm in diameter. The side cut for opening the flap was made by stepwise moving the laser focus in a circular arc of 345°, with 2-μm vertical separation between the lines. A part of the circle (15°) was left out from cutting to produce a hinge for folding the flap.

Imaging of Corneal Dissections

The cutting plane was imaged onto a charge-coupled device camera (Nikon D5100; Nikon, Tokyo, Japan) by combining the Zeiss microscope objective used for focusing the laser pulses into the corneal stroma with a Zeiss tube lens. The dissection zone was illuminated through a second microscope objective (Objective LD Plan-Neofluar 20×, NA 0.5; Carl Zeiss Microscopy) with light from a white light-emitting

diode placed below the cornea holder. Immediately (<1 minute) after the flap was cut, photographs of the cutting area were taken to determine the amount of gas bubble formation during the dissection process. In addition, an overview picture of the entire cornea after flap cutting and removing the cornea holder from the stage was photographed using a stereo microscope (Zeiss OPMI 1) and a digital camera (LEGRIA HF R18; Canon, Tokyo, Japan).

Determination of Laser Pulse Energy Required for Flap Cutting

The laser pulse energy at the laser focus was measured during each cut using an Ophir PD10-V2 energy meter (Ophir Optronics, Jerusalem, Israel). It was precalibrated without a microscope objective behind the aperture and taking into consideration the transmittance (T) of the Zeiss objective at 1030 nm ($T = 40\%$). To determine the laser pulse energy required for flap cutting, the pulse energy was, in a first step, adjusted to a level at which bubble formation in the corneal stroma became visible. The side cut was always performed at higher pulse energies to ensure a smooth cut. After flap cutting, the specimen was removed from the holder, and the flap was opened by an experienced surgeon using a hockey knife. The quality of the dissection was judged subjectively and classified into one of the three categories: (1) no flap lifting, (2) hard flap lifting, or (3) easy flap lifting. Depending on this classification, the laser pulse energy was then either increased or decreased to determine the minimum value required for easy flap lifting. This procedure was, at every laser pulse duration, repeated in 10 different corneas for both the Gaussian and the vortex beam (total number of investigated corneas = 60).

The irradiance threshold for plasma-induced bubble formation (also called laser-induced breakdown threshold) is known to be similar for water and ocular media.[25,26] Therefore, we use the threshold for plasma-induced bubble formation in water as a benchmark to assess the strength of mechanical effects in corneal dissection. A larger ratio between flap cutting threshold and bubble threshold implies more vigorous mechanical effects. Bubble thresholds in water at NA = 0.4 were determined in a different setup using a scattering technique described previously.[27–29]

Characterization of Cutting Quality

After successful flap dissection and lifting, the corneal specimens were fixated for 48 hours in fixing solution following the protocol of Graziadei et al.[30] The cornea was then prepared for scanning electron microscopy (SEM, Philips SEM 505; Philips, Amsterdam, Netherlands) by critical point drying and gold sputtering. The intrastromal cutting quality was characterized by the SEM images of the flap beds. The surface roughness in the SEM images was assessed using software designed for roughness analysis. We used the SurfChar plugin for ImageJ (National Institutes of Health, Bethesda, MD), which was designed according to ISO 25178 standard.[31] The software was originally designed to evaluate topographical information obtained through stereo-SEM, where picture pairs are taken under different angles; however, it is useful also for the analysis of individual SEM pictures.[32] Brightness contrast in SEM relies on the fact that the secondary electrons are detected under an oblique angle such that height variations are transformed into brightness variations.[20] Analysis of the local brightness fluctuations thus provides information on the roughness but in arbitrary units (AU) rather than on an absolute length scale.

Determination of Absorbed Laser Energy

For determining the laser pulse energy absorbed during intrastromal cutting, the transmitted laser light was collected with a second Zeiss microscope objective (NA 0.5) that was confocally and collinearly aligned to the focusing objective (NA 0.38). The larger NA of the second objective ensured that forward scattered light was also collected. The transmitted laser light was reflected by a dichroic mirror onto an energy meter (Ophir PE10 or PD10, depending on transmitted energy). To account for light losses by reflections at optical surfaces and absorption in the cornea, the energy meter behind the cornea was calibrated against the reference energy meter in the initial beam path (Fig. 2), and it was assumed that well below the energy required for flap cutting 100% of the incident light is transmitted through the laser focus. The incident laser pulse energy was stepwise increased from subthreshold values to higher energies leading to strong bubble formation. A large spot distance of 250×200 μm in the raster pattern was used to avoid interactions with larger bubbles from previous laser pulses at large pulse energies well above the bubble threshold. For this purpose, the translation stage was moved with 1 mm/s at a low laser repetition rate of 4 Hz. The absorbed energy (E_{abs}) was calculated from the measured values of incident energy (E_{in}) and the transmitted energy (E_T) by $E_{abs} = E_{in} - E_T$.
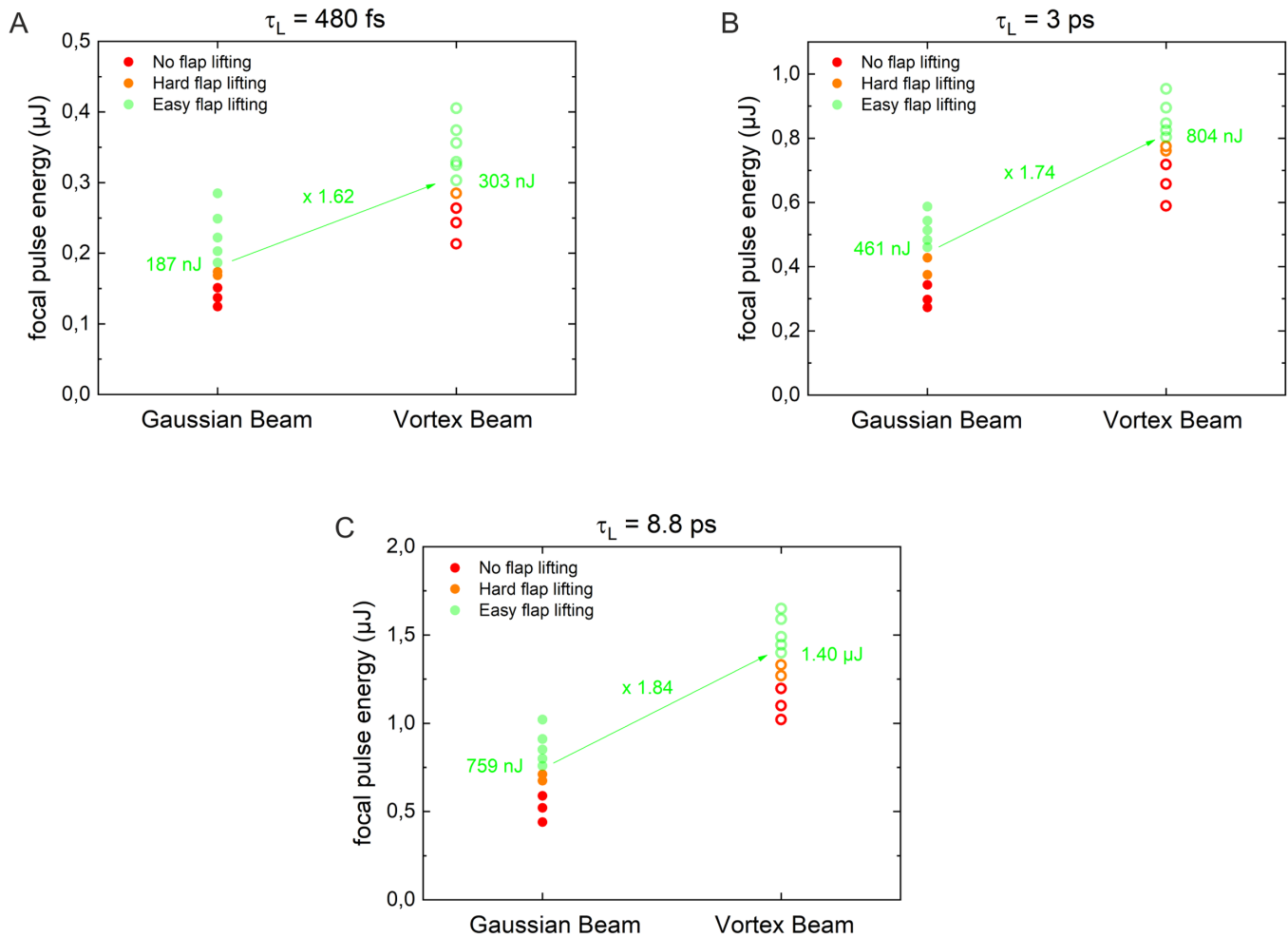
Figure 3. Classification of flap cuts at different laser pulse energies for Gaussian (*dots*) and vortex (*circles*) beams at laser pulse durations of (**A**) 480 fs, (**B**) 3 ps, and (**C**) 8.8 ps. Cutting attempts where no flap lifting was possible are marked in *red*, hard flap lifting in *orange*, and easy flap lifting in *green*. For each measurement series, the lowest energy value for which easy flap lifting could be achieved is indicated next to the corresponding data point.

Results

Laser Pulse Energy Required for Intrastromal Flap Cutting

Figure 3 summarizes the results of the measurement series performed to determine the laser pulse energy required for intrastromal flap cutting with Gaussian and vortex beams at different pulse durations. At all investigated pulse durations, the pulse energies required for flap cutting were a factor of 1.6 to 1.8 higher with the larger ring focus of the vortex beam than with the Gaussian beam. The threshold energy for flap cutting ($E_{th,cut}$) decreased significantly with decreasing pulse duration. For Gaussian beams it dropped

from 759 nJ at 8.8 ps to 187 nJ at 480 fs, and for vortex beams it decreased from 1.4 µJ at 8.8 ps to 303 nJ at 480 fs. The highest cutting quality with least disruptive side effects is expected at the lowest $E_{th,cut}$ values; therefore, a detailed characterization of the cutting quality was performed for the pulse duration of 480 fs.

SEM Images

Figure 4 shows representative SEM images of the flap beds in porcine corneas produced with 480-fs pulses at energies slightly above $E_{th,cut}$. At low magnification (Fig. 4A), the entire flap bed and a part of the flap are clearly visible. The edge of the flap bed
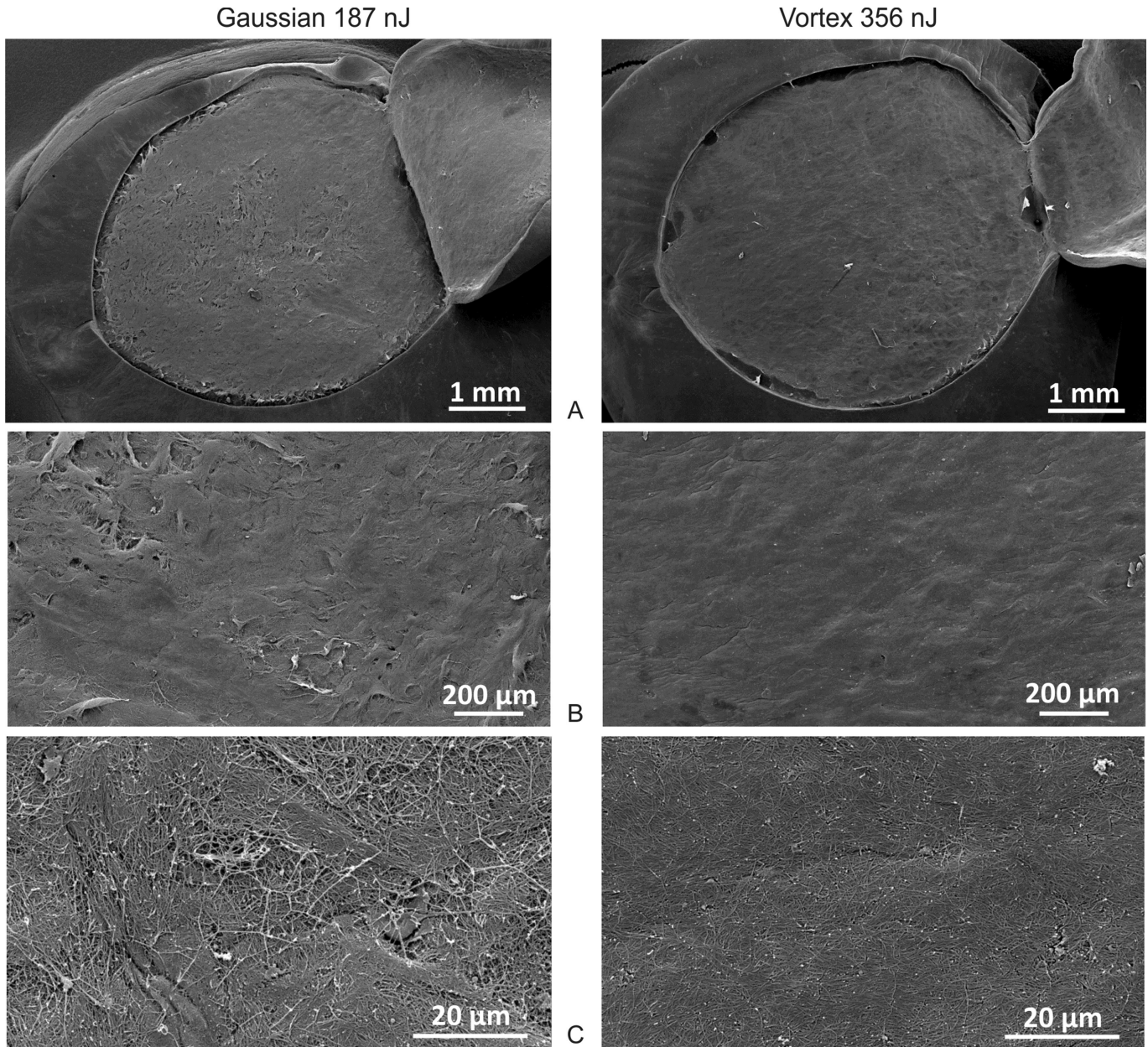
Gaussian 187 nJ   Vortex 356 nJ

Figure 4. SEM images of 6-mm flaps in porcine cornea that were cut using Gaussian (*left column*) and vortex (*right column*) beams with 1030-nm wavelength and 480-fs laser pulse duration. Pulse energies were slightly above the threshold for easy flap lifting.

shows some imperfections due to the higher laser pulse energy used for the side cut. The quality of the flap cuts can be determined by the surface roughness of the flap beds, visible at higher magnification (Figs. 4B, 4C). For the vortex beam, the flap bed is much smoother, with fewer irregularities along the lamellar structure of the cornea, than for the Gaussian beam. Average surface roughness is characterized by the arithmetic mean height deviation (S_a), which amounted to 14.90 versus 9.97 AU for the Gaussian and vortex beams in Figure 4B, and 29.25 versus 18.31 AU in Figure 4C, respectively.

Bubble Layer After Flap Cutting

Figure 5 shows the bubble layer after flap cutting with 480-fs, 1030-nm laser pulses, applied at a spot separation of 6×6 µm. Hardly any gas bubble formation was observed with the vortex beam, although the flap could be easily lifted. At high magnification, only the raster pattern of the laser foci was visible. By contrast, the Gaussian pulses produced a dense bubble layer. Already 1 minute after dissection small bubbles had coalesced; therefore, individual bubbles are visible also at low magnification under the stereo microscope.
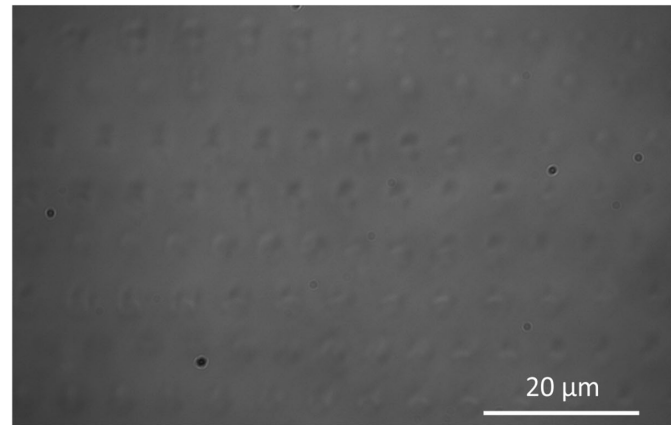
Gaussian 187 nJ
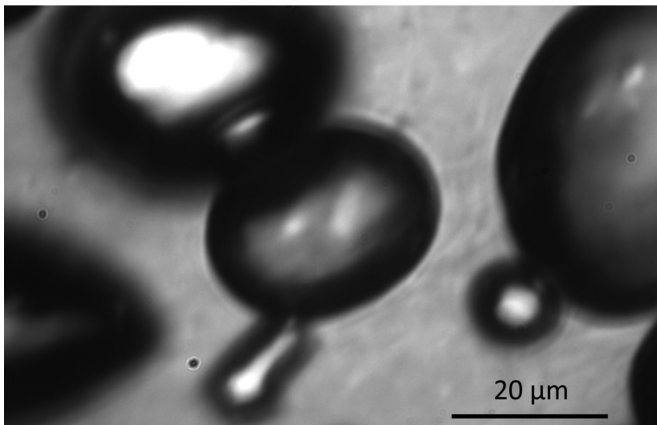
Vortex 303 nJ

Figure 5. Photographs of the laser-induced gas bubble layer after flap dissection with Gaussian (*left column*) and vortex (*right column*) beams with 1030-nm wavelength and 480-fs laser pulse duration. Photographs in the *upper row* were taken through the focusing objective less than 1 minute after flap cutting. Photographs in the *lower row* were taken 10 minutes after flap cutting using a stereo microscope.

Dissection Thresholds in Comparison to Bubble Thresholds in Water

Figure 6 shows the thresholds for flap cutting in cornea in comparison to bubble thresholds in water for Gaussian and vortex beams of different pulse durations. For the Gaussian beam, the energy required for flap cutting was always significantly higher than the bubble threshold in water (+76% at 480 fs, +56% at 3 ps, and +48% at 8.8 ps). In contrast, the vortex beam achieved cutting with energies very close to the bubble threshold (+1.0% at 480 fs, +8.6% at 3 ps, and +2.9% at 8.8 ps).

Absorbed Laser Energy During Intrastromal Flap Cutting

Figure 7 shows the dependence of laser energy transmission during intrastromal cutting on the incident laser pulse energy, and Figure 8 presents the absorbed energy at $E_{th,cut}$. Below the
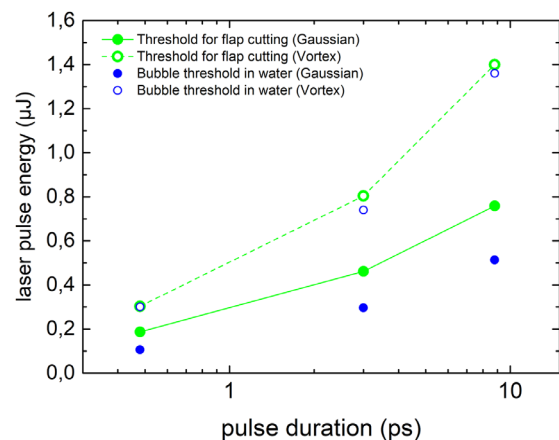

Figure 6. Thresholds for flap cutting (*green*) and bubble formation in water (*blue*) for Gaussian (*dots*) and vortex (*circles*) beams at 1030-nm wavelength and pulse durations of 480 fs, 3 ps, and 8.8 ps. NA = 0.38 in cornea; NA = 0.4 in water.

threshold for visible bubble formation in cornea, the transmission through the porcine cornea stayed
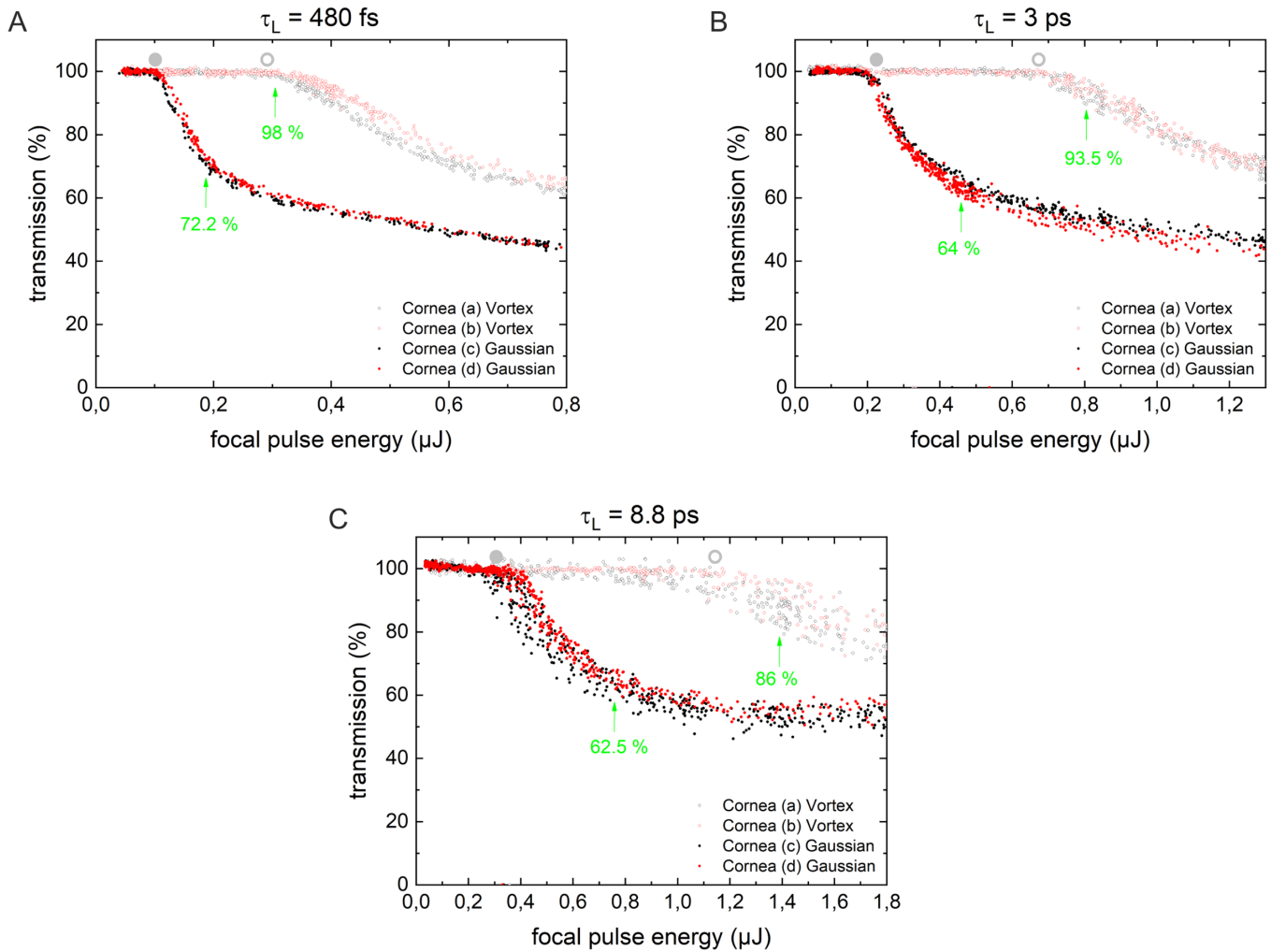
Figure 7. Laser energy transmission during intrastromal flap cutting for Gaussian and vortex beams at laser pulse durations of (**A**) 480 fs, (**B**) 3 ps, and (**C**) 8.8 ps. For each parameter set, two different porcine corneas were investigated (*red* and *black dots*). The thresholds for visible bubble formation in cornea are shown as *gray dots* (Gaussian) and *gray circles* (vortex). The energy values required for flap cutting are marked with *green arrows*, and the corresponding transmission values are indicated.
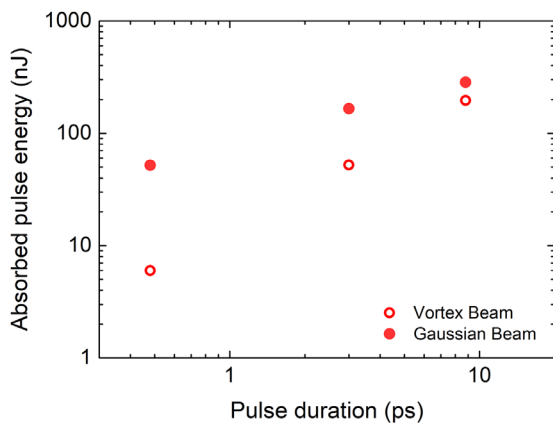

Figure 8. Absorbed laser pulse energy at $E_{th,cut}$ during flap cutting in porcine cornea with Gaussian (*dots*) and vortex (*circles*) beams.

constant at 100%. After bubble formation sets in, the transmission decreased with increasing laser pulse energy, because ever more laser energy was absorbed and converted into mechanical energy of the bubbles and acoustic transients. At $E_{th,cut}$, the transmission for the Gaussian beam was 72.2% at 480 fs, 64.0% at 3 ps, and 62.5% at 8.8 ps, corresponding to absorbed energy fractions of 27.8%, 36.0%, and 37.5%. For the vortex beam, the energy for flap cutting was higher than for the Gaussian beam, but the percentage of absorbed energy was much lower. We found transmission values of 98.0% at 480 fs, 93.5% at 3 ps, and 86.0% at 8.8 ps, corresponding to absorbed fractions of only 2.0%, 6.5%, and 14%. Figure 8 shows that the absolute values for E_{abs} were also lower for the vortex beam. The difference became larger with decreasing pulse duration, and at 480 fs the

absorbed energy values were 6 nJ for the vortex beam versus 52 nJ for the Gaussian beam.

Discussion

Cutting Efficiency and Precision

Our results show that focus shaping using vortex laser beams is a promising approach for gentle and ultraprecise intrastromal flap cutting in refractive surgery. Dissection of the transparent cornea is based on plasma formation by nonlinear energy deposition, also called laser-induced optical breakdown (LIOB).[4,18,33] Scanning the corneal stroma in a raster pattern at the same cutting depth produces many individual micro-explosions and cavitation bubbles, and their combined action finally leads to a cleavage plane. Tissue bridges arise where bubbles from neighboring plasmas do not meet. At equal spot distance within the 6-μm raster pattern, the part of the cleave plane covered by laser plasmas is larger for the vortex beam than for the Gaussian beam, and the reduced distance between the periphery of individual plasmas makes it easier for cleavage lines from neighboring foci to meet.[24] This reduces the number of tissue bridges arising from collagen fiber branching in the anterior cornea,[34] enhances the cutting efficiency, and improves the smoothness and precision of the cut (Fig. 4).

Although many researchers use a scoring system to support the subjective assessment of the surface properties of intrastromal dissections,[35–37] we followed the approach by Sarayba et al.,[32] who employed specialized software designed for roughness analysis. The results of the automated methodology confirmed the subjective impression gained from the SEM images, which favors cuts by the vortex beam.

For all investigated pulse durations, the incident energy (E_{in}) required for flap cutting was larger for the vortex beam than for the Gaussian beam (Fig. 3) because LIOB is an irradiance-dependent process, and the area of the ring-shaped focus is four times larger than the Gaussian focus. However, the real parameter governing both the efficiency and disruptiveness of dissection is the absorbed energy E_{abs} rather than E_{in}. The value of this parameter was dramatically reduced by using the ring-shaped focus (Fig. 7). At 480-fs pulse duration, E_{abs} at the flap cutting threshold was only 6 nJ energy per pulse with the vortex beam but was 52 nJ (8.7 times higher) for the Gaussian beam.

For a better assessment of the cutting efficiency, we compared the energy needed to mechanically separate corneal lamellae with the energy required for corneal dissection at different irradiation parameters. Smolek

and McCarey[38] determined the tearing force required to separate corneal lamellae at 50% stromal depth in 16 human eye bank corneas. Traction was applied perpendicular to the orientation of the lamellae, which minimizes the tearing work. The mean force needed to separate a 1-cm-wide strip was 0.142 kp = 1.39 N. The corresponding tearing work for a strip of 1- cm length was $1.39 \cdot 10^{-2}$ J, and the separation energy per unit area was $E_{sep} = 1.39 \cdot 10^{-2}$ J/cm². In our study, 6 nJ deposited energy per laser pulse was necessary for flap cutting with the vortex beam at 480-fs pulse duration and 6 μm × 6 μm spot separation. The corresponding energy per unit area was $E_{Flap,vortex} = 1.67 \cdot 10^{-2}$ J/cm², just 20% above the separation energy by tearing. Hence, corneal dissection using a vortex beam and appropriate spot separation is energetically close to the value achievable with mechanical tearing. With a Gaussian beam, the deposited energy per unit area required for flap dissection was $E_{Flap,Gaussian} = 14.5 \cdot 10^{-2}$ J/cm² and therefore 10.4 times larger compared to mechanical tearing, which is much less efficient than flap cutting using the vortex approach and may cause more disruption and mechanical side effects.

Mechanical Side Effects

Cutting energies are always well above the bubble threshold with Gaussian beams but close to the bubble threshold with vortex beams (Figs. 5, 6). This suggests that not only E_{abs} but also the plasma energy density are significantly lower for vortex beams. For ultrashort laser pulses, energy deposition is stress confined, and thermoelastic stress lowers the bubble threshold well below the superheat limit.[18,39] We conclude that the ring-shaped focus of the vortex beam facilitates cleavage along the corneal lamellae to such a degree that an explosive vaporization is not necessary for dissection but the thermoelastic stress produced at the bubble threshold is sufficient. As a consequence, cutting is less disruptive and mechanical side effects will be smaller.

In the following, we assess the mechanical stress on keratocytes close to the cut and on epithelial cells approximately 100 μm from the dissection plane (as often used clinically) for the shortest investigated pulse duration, 480 fs, which produced the smoothest cuts with least energy. For femtosecond breakdown at the bubble threshold, Vogel and coworkers[18] obtained a theoretical prediction of 42 MPa for the amplitude of the thermoelastic stress wave at the plasma rim and experimental values between 56 and 61 MPa by back-extrapolation of far-field hydrophone measurements. With a vortex beam, flap dissections are performed
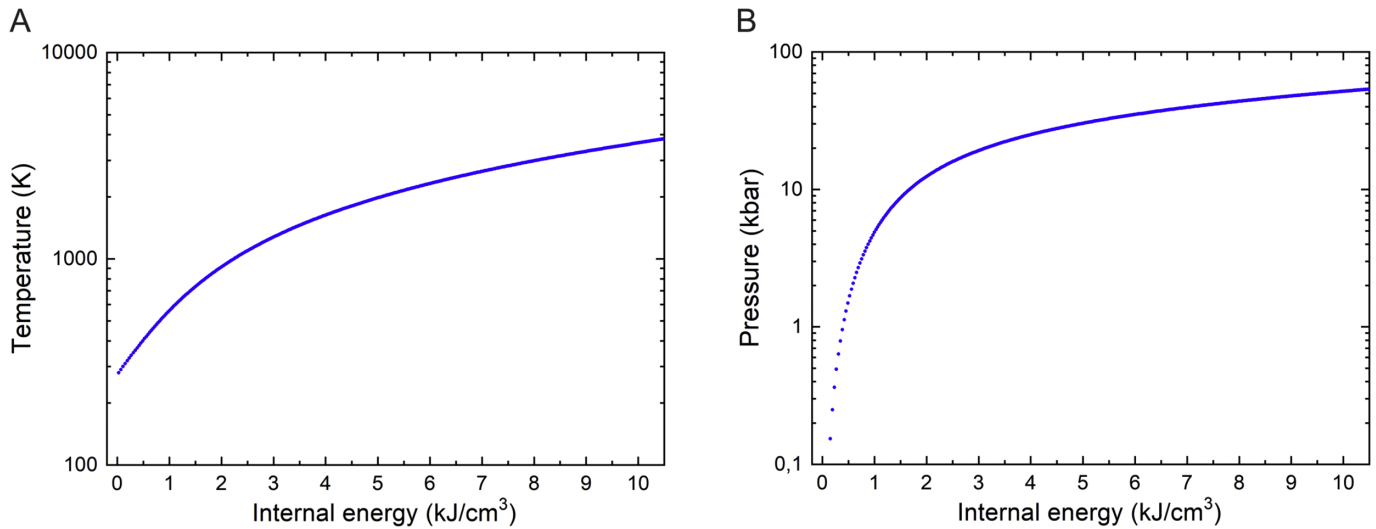
A

B

Figure 9. Temperature (**A**) and pressure (**B**) as a function of internal energy for a mass density $\rho_0 = 1000$ kg m^{-3}, according to the IAPWS-95 formulation of the EOS of water.[41]

very close to the bubble threshold (Figs. 6, 7), and we can thus assume peak pressures of about 50 MPa in the immediate vicinity of the cut. The pressure decays with scaling law $p \propto r^n$, with $n = 1.12$,[18,40] which results in a pressure of 0.57 MPa at a distance of 100 µm when considering a plasma radius of 1.83 µm, which is smaller than the ring focus radius of 3.0 µm because of the sixth-order multiphoton ionization process involved in the plasma formation process.[18]

With a Gaussian beam of 480-fs pulses, the pressure at the plasma rim is much higher. The incident energy required for flap cutting was 76% larger than the bubble threshold $E_{th,bubble}$, but the absorbed energy was even 8.7 times larger than for the vortex beam. The ratio of plasma energy densities (U) depends on the ratio of absorbed energies and on the respective plasma volumes. The focal diameter is smaller for the Gaussian beam, but the plasma length at $1.76 \times E_{th,bubble}$ is larger than for flap cutting with the vortex beam occurring close to $E_{th,bubble}$. Because a precise quantification of the plasma volumes is difficult, we roughly estimated a plasma energy density ratio ($U_{Gaussian}/U_{vortex}$) of 10 to 15. Energy deposition in femtosecond breakdown is isochoric[18] (i.e., volume and mass density remain constant during heating), and the relations among internal energy, temperature, and pressure are unambiguously determined by the equation of state (EOS) of the material. Because tissue consists mostly of water, we used the International Association for the Properties of Water and Steam 1995 (IAPWS-95) formulation of the water EOS[41] to determine the peak plasma pressure for the Gaussian beam at the flap cutting threshold (Fig. 9).

Our calculations are based on the finding from Vogel et al.[18] that at the bubble threshold the temperature at the focus center rises by 131.5°C, corresponding to an internal energy gain of 0.50 kJ/cm^3. We assume that the same holds for the bubble and flap cutting threshold of the vortex beam. With the Gaussian beam, the internal energy at the cutting threshold is 10 to 15 times larger than at the bubble threshold and amounts to 5.0 to 7.5 kJ/cm^3. This results in peak temperatures of 2000°C to 2850°C and peak pressures of 3000 to 4200 MPa. The pressure at the plasma rim is approximately 25% of the maximum compressive amplitude at the focus center (see figure 14 in Vogel et al.[18]) and amounts to 750 to 1050 MPa. The corresponding pressure at the epithelium obtained using the scaling law $p \propto r^n$ with $n = 1.12$ and a plasma radius of 1.0 µm (value assumed for $1.76 \times E_{th,bubble}$) fall within the range of 4.3 to 6.0 MPa, more than 7.6 to 10.6 times larger than with the vortex beam.

Corneal cells are exposed not just to compressive stress but to a bipolar wave in which the compressive part is followed by tensile stress. This is partly a feature of the thermoelastic stress wave produced by isochoric energy deposition with ultrashort laser pulses,[18,42] but in corneal tissue it is also a general feature arising from the elastic tissue response that is relevant also for longer (ns) pulses.[43] The threshold for cell death after exposure to individual shock waves is ≈50 MPa,[44,45] but the damage threshold for bipolar stress waves was found to be smaller, around 10 MPa for the peak tensile stress amplitude[45,46] because cells are more susceptible to tensile than to compressive stress.[47] These damage threshold data

suggest that, with a vortex beam, when the cutting threshold of the compressive pressure of the bipolar stress wave at the plasma rim is ≈50 MPa, damage is produced only in the immediate vicinity of the dissection plane. The corneal epithelium and also the endothelium, which is >300 μm away from the cut, are safe because the pressure amplitude at a distance of 100 μm is only ≈0.6 MPa. By contrast, the range of damage is much larger for the Gaussian beam, for which the pressure at the plasma rim is approximately 750 to 1050 MPa. Even in the epithelial layer, pressure amplitudes of approximately 4.3 to 6.0 MPa are reached, and each epithelial cell is exposed to about 50 pressure waves of similar amplitude because the laser pulses are applied in a raster pattern with a spot separation of only a few micrometers. Thus, there is a certain potential for epithelial damage induced by acoustic transient waves that may become relevant if combined with other stress factors.

In addition to the laser-induced stress transients, shear stress arising from cavitation bubble oscillations is another mechanical stress factor.[16,40,43,48] It is relevant in a zone reaching approximately up to the maximum bubble radius, which extends a few micrometers beyond the cutting plane (≤10 μm for $E_{pulse} \leq 1$ μJ with a Gaussian beam[17]). Beyond this range, stress-wave-induced damage will dominate.

The above assessment of the range of damage due to mechanical stress is corroborated by investigations on cell viability after flap dissections in rabbit eyes with a Gaussian beam that were based on ultrastructural analysis, detection of apoptosis by means of the TUNEL assay, and immunocytochemistry.[49,50] The width of the apoptotic zone was found to be ≈20 μm for $E_{pulse} = 0.5$ μJ and increased to ≈60 μm for $E_{pulse} = 2.7$ μJ.[50] We hypothesize that the pronounced reduction of mechanical stress due to the lower pressure amplitudes and the diminished cavitation will markedly reduce early keratocyte apoptosis and necrosis. This could lead to diminished keratocyte proliferation and myofibroblast generation later in the wound-healing process,[51] which would improve the clinical outcome and predictability of refractive procedures and may further reduce haze.

Bubble Layer After Dissection

Cutting with vortex beam occurs close to the bubble threshold. Because in ultrashort-pulse optical breakdown, the phase transition at bubble threshold is facilitated by thermoelastic tensile stress, the threshold temperature is lowered to ≈150°C compared to ≈300°C for explosive vaporization

without stress confinement.[18,29] As a consequence, relatively little liquid is vaporized at threshold, and the amount of non-condensable gas resulting from free-electron-mediated molecular fragmentation is also small. This explains the lack of long-lived gas bubbles in dissections produced with the vortex beam (Fig. 5, right column).

With a Gaussian beam, the absorbed energy is 1.45 times ($\tau_L = 8.8$ ps) to 8.7 times ($\tau_L = 480$ fs) higher than with the vortex beam, and the focal volume is much smaller. Therefore, the plasma density and temperature rise in the focal volume are much greater, as discussed above, and peak temperatures can well exceed 1000°C. This favors free-electron-mediated molecular disintegration as well as pyrolysis and explains the large amount of non-condensable gas that forms the layer of long-lived gas bubbles[18,52–55] (Fig. 5, left column).

Pulse Duration Dependence of Cutting Energy

A decrease of the pulse duration from 8.8 ps to 480 fs results in a reduction of the absorbed laser pulse energy required for flap cutting by a factor of 5.5 for the Gaussian beam and by a factor of 32 for the vortex beam (Fig. 8). This result is remarkable and not easy to understand. A possible explanation for the higher dissection efficiency of femtosecond breakdown could be linked to an increasing degree of stress confinement with decreasing pulse duration. Plasma-mediated heating occurs by thermalization of the energy of the free electrons via collisions and recombinations. At plasma densities leading to bubble formation, this process is completed within 10 to 20 ps,[28,56] which is comparable to the longest laser pulse duration investigated in this study. Thermal expansion of the focal volume takes much longer and is completed when the expansion wave traveling at sound velocity has propagated through the heat source, which takes 660 ps for a plasma with 1-μm diameter (sound velocity $c_s = 1480$ m/s). Thus, energy deposition is isochoric and compressive thermoelastic stress builds up during heating.[18,39] However, because the energy deposition was "stress confined" for all pulse durations investigated in this study, different degrees of stress confinement cannot explain the observed dependence of cutting energy on pulse duration.

We hypothesize that the variations of cutting efficiency are related to differences in the plasma absorption coefficient leading to different peak pressures at the same absorbed energy. This conjecture is supported by transmission measurements,

which showed a peak of plasma transmission at pulse durations of a few picoseconds and a decrease of transmission when the pulse duration τ_L was shortened into the femtosecond range.[57] Numerical simulations of Noack and Vogel[58] revealed that the time-averaged plasma absorption coefficient during a laser pulse first decreases when τ_L drops below 1 ns, assumes a minimum for pulse durations of a few picoseconds, and increases again for femtosecond breakdown. The calculations showed that, for the picosecond pulses, a high electron density is reached only late during the laser pulse, after its irradiance maximum is surpassed, which diminishes absorption. The absorption coefficient grows in the femtosecond domain, because the increasingly strong generation of free electrons by multiphoton absorption results in an early rise of the free electron density, which is then amplified by avalanche ionization $\propto \rho \times I$. As a consequence of the higher time-averaged absorption coefficient at $\tau_L = 480$ fs, the plasma volume into which a given amount of laser energy is absorbed is smaller than for the picosecond pulses; therefore, the energy density and plasma pressure are higher for a given laser pulse energy. This implies that the pressure values required for disruptive tissue dissection are reached at lower pulse energies for the shorter pulse durations. Future spatiotemporal simulations of plasma growth and plasma energy density distribution will be needed to confirm this hypothesis.[59–62]

Potential Improvements of Refractive Surgery by Focus Shaping

An opaque bubble layer in the anterior stroma during LASIK[63] is a well-known intraoperative finding seen with all clinical femtosecond laser systems.[7] An excessive opaque bubble layer can lead to complications during flap creation, and bubble remnants remaining in the corneal stroma after flap lifting may compromise residual stromal thickness measurements and the reliability of pupil tracking systems.[8,63] In rare cases, vertical gas breakthrough can occur when cavitation bubbles cleave lamella toward Bowman's layer and disrupt the epithelium. A vertical channel, a so-called buttonhole, is then created, and complications such as epithelial ingrowth and scarring can affect the outcome of the procedure.[9,64] Reduction of the opaque bubble layer when using a vortex beam can, therefore, greatly improve the dissection process.

The increased precision and reduction in mechanical side effects in intrastromal cutting by the use of a vortex beam make this a promising approach for flap cutting in LASIK[4] and intrastromal pocket dissection for hyperopia correction[13,14] and offers even greater potential for improving SMILE.[10] In SMILE, a small lenticule is dissected and removed through a small side cut to achieve refractive correction in one step. Formation of an opaque bubble layer is a known complication in SMILE.[65–67] Mechanical deformation of the corneal stroma by bubble formation during the lower cut may induce undesired local variations of the lenticule thickness, because the mechanical distortions of the corneal lamellae by cavitation affect a significantly larger volume than the plasma-induced tissue vaporization.[68,69] The decrease in bubble formation and mechanical stress enabled by the vortex approach, along with the improved cutting quality, could enhance the precision and predictability of SMILE.

Implementation of Focus Shaping into Clinical Systems

Like Gaussian beams, Laguerre–Gaussian vortex beams are propagation invariant; that is, after the phase plate the beam retains its vortex characteristics along the entire beam path. This feature enables easy implementation of the phase plate into a beam delivery system and is compatible with beam scanning after the plate. The phase plate can be easily swung in and out of the laser beam to switch between Gaussian and vortex beams.[24] Although the vortex beam is advantageous for lenticule cutting in SMILE and the flap bed in LASIK, the Gaussian beam, with its more elongated plasma shape, may be better suited for the vertical side cuts of the LASIK flap.

Alternative approaches for creating a ring focus do not have these advantages. A lens–axicon combination provides a ring focus at the focal plane of the lens,[70] but the z-location of the optical elements is critical, combining this technique with beam scanning is difficult, and the ring focus is longer than the Gaussian focus without an axicon because the effective NA in the optical system is halved by the use of an axicon. By contrast, the ring focus of a vortex beam has the same length as the Gaussian focus produced at equal NA. Beam shaping by diffractive or refractive optics can produce arbitrary intensity distributions in a plane of interest, which can also be the focal plane of a laser.[71] However, the z-location of the optical elements is again critical, and combining this technique with beam scanning is impossible. Moreover, intensity peaks ("hot spots") are usually located in front or behind of the plane with the desired intensity distribution, which compromises plasma-mediated cutting in a well-defined plane. In contrast, the creation of vortex

beams by insertion of a spiral phase plate is a simple, versatile, and cost-effective way of improving the efficiency and precision of intrastromal corneal dissections for LASIK and SMILE.

Conclusions

In an ex vivo study on porcine eyes, we explored possible improvements of intrastromal dissection by focus shaping using a helical phase plate. The resulting vortex beam had a ring focus with the same length as a Gaussian beam of equal NA but four times larger cross-section. The use of a vortex beam was found to improve the precision and efficiency of cuts and to reduce bubble formation in the cutting plane. These features are of interest for both LASIK and SMILE. Cutting with the vortex beam is less disruptive, and mechanical side effects are less severe than with conventional Gaussian beams. A reduction in early keratocyte apoptosis and necrosis could lead to diminished keratocyte proliferation and myofibroblast generation in the wound-healing process and may lower the incidence of diffuse lamellar keratitis. In SMILE, the refractive outcome largely relies on the precision of lenticule dissection. Bubble formation distorts the stromal morphology during cutting and compromises precision; thus, reduced bubble formation would improve the predictability of the surgical procedure. Because the phase plate for creating a helical phase can be implemented into the delivery systems of existing clinical device, the vortex beam approach can be easily tested in animal experiments and clinical trials. This could enable its use in the next generation of refractive laser systems.

Acknowledgments

References

1. Pallikaris IG, Papatzanaki ME, Stathi EZ, Frenschock O, Georgiadis A. Laser in situ keratomileusis. *Lasers Surg Med*. 1990;10:463–468.

2. Pallikaris IG, Papatzanaki ME, Siganos DS, Tsilimbaris MK. A corneal flap technique for laser in situ keratomileusis. Human studies. *Arch Ophthalmol*. 1991;109:1699–1702.

3. Buratto L, Ferrari M, Rama P. Excimer laser intrastromal keratomileusis. *Am J Ophthalmol*. 1992;113:291–295.

4. Juhasz T, Loesel F, Kurtz RM, Horvath C, Bille JF, Mourou G. Corneal refractive surgery with femtosecond lasers. *IEEE J Sel Top Quantum Electron*. 1999;5:902–910.

5. Lubatschowski H, Maatz G, Heisterkamp A, et al. Application of ultrashort laser pulses for intrastromal refractive surgery. *Graefes Arch Clin Exp Ophthalmol*. 2000;238:33–39.

6. Kohnen T, Strenger A, Klaproth OK. Basic knowledge of refractive surgery: correction of refractive errors using modern surgical procedures. *Dtsch Arztebl Int*. 2008;105:163–170.

7. Shah DN, Melki S. Complications of femtosecond-assisted laser in-situ keratomileusis flaps. *Semin Ophthalmol*. 2014;29:363–375.

8. dos Santos AM, Torricelli AA, Marino GK, et al. Femtosecond laser-assisted LASIK flap complications. *J Refract Surg*. 2016;32:52–59.

9. Tucker SH, Sood P. Flap complications from femtosecond laser-assisted in situ keratomileusis. *US Ophthalmic Rev*. 2019;12:21–27.

10. Sekundo W, Kunert KS, Blum M. Small incision corneal refractive surgery using the small incision lenticule extraction (SMILE) procedure for the correction of myopia and myopic astigmatism: results of a 6 month prospective study. *Br J Ophthalmol*. 2011;95:335–339.

11. Guell JL, Verdaguer P, Mateu-Figueras G, et al. SMILE procedures with four different cap thicknesses for the correction of myopia and myopic astigmatism. *J Refract Surg*. 2015;31:580–585.

12. Blum M, Taubig K, Gruhn C, Sekundo W, Kunert KS. Five-year results of small incision lenticule extraction (ReLEx SMILE). *Br J Ophthalmol*. 2016;100:1192–1195.

13. Freidank S, Vogel A, Anderson RR, Birngruber R, Linz N. Correction of hyperopia by intrastromal cutting and liquid filler injection. *J Biomed Opt*. 2019;24:058001.

14. Wertheimer CM, Brandt K, Kaminsky S, et al. Refractive changes after corneal stromal filler injection for the correction of hyperopia. *J Refract Surg*. 2020;36:406–413.

15. Zuberbuhler B, Tuft S, Gartry D, Spokes D. *Corneal Surgery*. Berlin: Springer; 2013:146.

16. Vogel A, Asiyo-Vogel M, Birngruber R. Investigations on intrastromal refractive surgery with

picosecond Nd-Yag laser-pulses. *Invest Ophthalmol Vis Sci*. 1994;35:2155.

17. Juhasz T, Kastis GA, Suarez C, Bor Z, Bron WE. Time-resolved observations of shock waves and cavitation bubbles generated by femtosecond laser pulses in corneal tissue and water. *Lasers Surg Med*. 1996;19:23–31.

18. Vogel A, Noack J, Huttman G, Paltauf G. Mechanisms of femtosecond laser nanosurgery of cells and tissues. *Appl Phys B*. 2005;81:1015–1047.

19. Lubatschowski H. Overview of commercially available femtosecond lasers in refractive surgery. *J Refract Surg*. 2008;24:102–107.

20. Murphy DB, Davidson MW. *Fundamentals of Light Microscopy and Electronic Imaging*. 2nd ed. Hoboken, NJ: Wiley-Blackwell; 2012:560.

21. Yao AM, Padgett MJ. Orbital angular momentum: origins, behavior and applications. *Adv Opt Photon*. 2011;3:161–204.

22. HOLO/OR, Ltd. Optical Vortex Phase Plate. Available at: https://www.holoor.co.il/application/optical-vortex-phase-plate-application-notes/. Accessed September 15, 2020.

23. Hao XA, Kuang CF, Wang TT, Liu X. Effects of polarization on the de-excitation dark focal spot in STED microscopy. *J Opt*. 2010;12:115707.

24. Vogel A, Freidank S, Linz N, inventors. Device for laser cutting within transparent materials. European Patent 2760622 B1, US Patent 9795511 B2, Chinese Patent 104703563 B, Japanese Patent 6005290 B2. 2015.

25. Docchio F, Sacchi C, Marshall J. Experimental investigation of optical breakdown thresholds in ocular media under single pulse irradiation with different pulse durations. *Lasers Ophthalmol*. 1986;1:82–93.

26. Linz N, Freidank S, Liang XX, Vogel A. Experimental and theoretical investigation of the mechanisms of free-electron-mediated modification of biomolecules in nonlinear microscopy, AFOSR-FA9550-15-1-0326, AFOSR Biophysics Program Review 2018-04-20. Luebeck, Germany: Institute of Biomedical Optics, University of Luebeck; 2018.

27. Linz N, Freidank S, Liang XX, Vogelmann H, Trickl T, Vogel A. Wavelength dependence of nanosecond infrared laser-induced breakdown in water: evidence for multiphoton initiation via an intermediate state. *Phys Rev B*. 2015;91:134114.

28. Linz N, Freidank S, Liang XX, Vogel A. Wavelength dependence of femtosecond laser-induced breakdown in water and implications for laser surgery. *Phys Rev B*. 2016;94:024113.

29. Vogel A, Linz N, Freidank S, Paltauf G. Femtosecond-laser-induced nanocavitation in water: implications for optical breakdown threshold and cell surgery. *Phys Rev Lett*. 2008;100:038102.

30. Graziadei GAM, Graziadei PPC. Neurogenesis and neuron regeneration in the olfactory system of mammals. 2. Degeneration and reconstitution of the olfactory sensory neurons after axotomy. *J Neurocytol*. 1979;8:197–213.

31. Chinga G, Johnsen PO, Dougherty R, Berli EL, Walter J. Quantification of the 3D microstructure of SC surfaces. *J Microsc*. 2007;227:254–265.

32. Sarayba MA, Ignacio TS, Binder PS, Tran DB. Comparative study of stromal bed quality by using mechanical, IntraLase femtosecond laser 15- and 30-kHz microkeratomes. *Cornea*. 2007;26:446–451.

33. Sander M, Stolte A, Müller M, Lochmann C, Tetz MR. Monitoring the cutting process of the laser-induced optical breakdown (LIOB) during femtosecond-laser in-situ keratomileusis (fs-LASIK). *Med Laser Appl*. 2009;24:158–164.

34. Winkler M, Chai D, Kriling S, et al. Nonlinear optical macroscopic assessment of 3-D corneal collagen organization and axial biomechanics. *Invest Ophthalmol Vis Sci*. 2011;52:8818–8827.

35. Wilhelm FW, Giessmann T, Hanschke R, Duncker GI, Wilhelm LH. Cut edges and surface characteristics produced by different microkeratomes. *J Refract Surg*. 2000;16:690–700.

36. Kunert KS, Blum M, Duncker GI, Sietmann R, Heichel J. Surface quality of human corneal lenticules after femtosecond laser surgery for myopia comparing different laser parameters. *Graefes Arch Clin Exp Ophthalmol*. 2011;249:1417–1424.

37. Ziebarth NM, Lorenzo MA, Chow J, et al. Surface quality of human corneal lenticules after SMILE assessed using environmental scanning electron microscopy. *J Refract Surg*. 2014;30:388–393.

38. Smolek MK, McCarey BE. Interlamellar adhesive strength in human eyebank corneas. *Invest Ophthalmol Vis Sci*. 1990;31:1087–1095.

39. Vogel A, Venugopalan V. Mechanisms of pulsed laser ablation of biological tissues. *Chem Rev*. 2003;103:577–644.

40. Vogel A, Busch S, Parlitz U. Shock wave emission and cavitation bubble generation by picosecond and nanosecond optical breakdown in water. *J Acoust Soc Am*. 1996;100:148–165.

41. Wagner W, Pruss A. The IAPWS formulation 1995 for the thermodynamic properties of ordinary water substance for general and scientific use. *J Phys Chem Ref Data*. 2002;31:387–535.

42. Paltauf G, Schmidt-Kloiber H. Photoacoustic cavitation in spherical and cylindrical absorbers. *Appl Phys A*. 1999;68:525–531.

43. Brujan EA, Vogel A. Stress wave emission and cavitation bubble dynamics by nanosecond optical breakdown in a tissue phantom. *J Fluid Mech*. 2006;558:281–308.

44. Doukas AG, McAuliffe DJ, Flotte TJ. Biological effects of laser-induced shock waves: structural and functional cell damage in vitro. *Ultrasound Med Biol*. 1993;19:137–146.

45. Doukas AG, Flotte TJ. Physical characteristics and biological effects of laser-induced stress waves. *Ultrasound Med Biol*. 1996;22:151–164.

46. Esenaliev RO, Golovlyova OA, Golovlyov VV, Letokhov VS. Effect on erythrocytes of acoustic waves generated upon absorption of laser radiation. *Lasers Life Sci*. 1994;6:153–161.

47. Duck FA. *Physical Properties of Tissue*. London: Academic Press; 1990.

48. Gaudron R, Warnez MT, Johnsen E. Bubble dynamics in a viscoelastic medium with nonlinear elasticity. *J Fluid Mech*. 2015;766:54–75.

49. Netto MV, Mohan RR, Medeiros FW, et al. Femtosecond laser and microkeratome corneal flaps: comparison of stromal wound healing and inflammation. *J Refract Surg*. 2007;23:667–676.

50. de Medeiros FW, Kaur H, Agrawal V, et al. Effect of femtosecond laser energy level on corneal stromal cell death and inflammation. *J Refract Surg*. 2009;25:869–874.

51. Mohan RR, Hutcheon AEK, Choi R, et al. Apoptosis, necrosis, proliferation, and myofibroblast generation in the stroma following LASIK and PRK. *Exp Eye Res*. 2003;76:71–87.

52. Lim JJ, Shamos MH. Evaluation of kinetic parameters of thermal decomposition of native collagen by thermogravimetric analysis. *Biopolymers*. 1974;13:1791–1807.

53. McKenzie AL. A three-zone model of soft-tissue damage by a CO_2 laser. *Phys Med Biol*. 1986;31:967–983.

54. Maatz G, Heisterkamp A, Lubatschowski H, et al. Chemical and physical side effects at application of ultrashort laser pulses for intrastromal refractive surgery. *J Opt Soc Am A*. 2000;2:59–64.

55. Vogel A, Venugopalan V. Pulsed laser ablation of tissue. In: Welch AJ, van Gemert M, eds. *Optical-Thermal Response of Laser-Irradiated Tissue*. 2nd ed. Heidelberg, NY: Springer; 2011:551–614.

56. Schaffer CB, Nishimura N, Glezer EN, Kim AMT, Mazur E. Dynamics of femtosecond laser-induced breakdown in water from femtoseconds to microseconds. *Opt Express*. 2002;10:196–203.

57. Vogel A, Noack J, Nahen K, et al. Energy balance of optical breakdown in water at nanosecond to femtosecond time scales. *Appl Phys B*. 1999;68:271–280.

58. Noack J, Vogel A. Laser-induced plasma formation in water at nanosecond to femtosecond time scales: calculation of thresholds, absorption coefficients, and energy density. *IEEE J Quantum Electron*. 1999;35:1156–1167.

59. Arnold CL, Heisterkamp A, Ertmer W, Lubatschowski H. Computational model for nonlinear plasma formation in high NA micromachining of transparent materials and biological cells. *Opt Express*. 2007;15:10303–10317.

60. Bulgakova NM, Zhukov VP, Sonina SV, Meshcheryakov YP. Modification of transparent materials with ultrashort laser pulses: what is energetically and mechanically meaningful? *J Appl Phys*. 2015;118:233108.

61. Jukna V, Jarnac A, Milian C, et al. Underwater acoustic wave generation by filamentation of terawatt ultrashort laser pulses. *Phys Rev E*. 2016;93:063106.

62. Fedorov VY, Chanal M, Grojo D, Tzortzakis S. Accessing extreme spatiotemporal localization of high-power laser radiation through transformation optics and scalar wave equations. *Phys Rev Lett*. 2016;117:043902.

63. Liu CH, Sun CC, Hui-Kang Ma D, et al. Opaque bubble layer: incidence, risk factors, and clinical relevance. *J Cataract Refract Surg*. 2014;40:435–440.

64. Harissi-Dagher M, Todani A, Melki SA. Laser in situ keratomileusis buttonhole: classification and management algorithm. *J Cataract Refract Surg*. 2008;34:1892–1899.

65. Mastropasqua L, Calienno R, Lanzini M, et al. Opaque bubble layer incidence in femtosecond laser-assisted LASIK: comparison among different flap design parameters. *Int Ophthalmol*. 2017;37:635–641.

66. Son G, Lee J, Jang C, Choi KY, Cho BJ, Lim TH. Possible risk factors and clinical effects of opaque bubble layer in small incision lenticule extraction (SMILE). *J Refract Surg*. 2017;33:24–29.

67. Li L, Schallhorn JM, Ma J, Zhang L, Dou R, Wang Y. Risk factors for opaque bubble layer in small incision lenticule Extraction (SMILE). *J Refract Surg*. 2017;33:759–764.

68. Vogel A, Capon MRC, Asiyo-Vogel MN, Birngruber R. Intraocular photodisruption with picosecond and nanosecond laser pulses: tissue effects in

cornea, lens, and retina. *Invest Ophthalmol Vis Sci.* 1994;35:3032–3044.

69. Vogel A, Gunther T, Asiyo-Vogel M, Birngruber R. Factors determining the refractive effects of intrastromal photorefractive keratectomy with the picosecond laser. *J Cataract Refract Surg.* 1997;23:1301–1310.

70. Belanger PA, Rioux M. Ring pattern of a lens-axicon doublet illuminated by a Gaussian-beam. *Appl Opt.* 1978;17:1080–1088.

71. Umhofer U, Jäger E, Bischoff C. Refractive and diffractive laser beam shaping optics. *Laser Technik J.* 2011;8:24–27.